Journal of Power Sources 196 (2011) 5591–5594

Contents lists available at ScienceDirect

Journal of Power Sources

journal homepage: www.elsevier.com/locate/jpowsour

Short communication

$NiMn_2O_4$ spinel as an alternative coating material for metallic interconnects of intermediate temperature solid oxide fuel cells

Wenying Zhang, Jian Pu*, Bo Chi, Li Jian

School of Materials Science and Engineering, State Key Laboratory of Material Processing and Die & Mould Technology, Huazhong University of Science & Technology, Wuhan, Hubei 430074, China

ARTICLE INFO

Article history:
Received 29 December 2010
Received in revised form 17 February 2011
Accepted 17 February 2011
Available online 26 February 2011

Keywords:
Solid oxide fuel cell
Metallic interconnect
Spinel $NiMn_2O_4$
Oxidation kinetics
Area specific resistance

ABSTRACT

In an effort to improve the performance of SUS 430 alloy as a metallic interconnect material, a low cost and Cr-free spinel coating of $NiMn_2O_4$ is prepared on SUS 430 alloy substrate by the sol–gel method and evaluated in terms of the microstructure, oxidation resistance and electrical conductivity. A oxide scale of 3–4 μm thick is formed during cyclic oxidation at 750 °C in air for 1000 h, consisting of an inner layer of doped Cr_2O_3 and an outer layer of doped $NiMn_2O_4$ and Mn_2O_3; and the growth of Cr_2O_3 and formation of $MnCr_2O_4$ are depressed. The oxidation kinetics obeys the parabolic law with a rate constant as low as 4.59×10^{-15} g^2 cm^{-4} s^{-1}. The area specific resistance at temperatures between 600 and 800 °C is in the range of 6 and 17 mΩ cm^2. The above results indicate that $NiMn_2O_4$ is a promising coating material for metallic interconnects of the intermediate temperature solid oxide fuel cells.

1. Introduction

The interconnect is a key component in a stack of planar solid oxide fuel cells (SOFCs), which physically separates the fuel and oxidant, provides electrical connection between cells and distributes reactant gases onto the electrodes. As SOFC operating temperature decreases from previously high temperature near 1000 °C to the intermediate temperature range of 600–800 °C, metallic alloys are considered as the candidate materials for the interconnect application [1–3] with potential advantages of high electrical/thermal conductivity, robust fabricability and structural integrity as well as significantly low material cost in comparison to their ceramic counterpart.

Among the oxidation resistant alloys, Cr_2O_3-forming ferritic stainless steels, such as SUS 430 and Crofer 22 [4,5], are favored as the candidate materials for the interconnects. These alloys form a well-adhered and dense inner scale of Cr_2O_3, which is conductive at the operating temperature and slows down further oxidation of the substrate, and a less dense outer scale of $(Cr,Mn)_3O_4$ spinel, which reduces Cr vaporization in the form of volatile Cr-containing species. However, the oxidation resistance of these ferritic stainless steels is not adequate for a long-term SOFC operation at the intermediate temperature, and the spinel $(Cr,Mn)_3O_4$ cannot fully prevent the cathode from being poisoned by the Cr evaporation [6,7]. Consequently, the area specific resistance (ASR) contributed by the metallic interconnect increases with time due to the growth of the oxide scale, while the cathode performance degrades due to the deposition of the volatile Cr species on the active surface of the cathode [8–10]. Therefore, it is a consensus that surface coating is needed for the conventional ferritic stainless steels that are to be used for the interconnects in the intermediate temperature SOFCs. Such coatings are required to be dense, electrically conductive, non-volatile and chemically compatible with other cell components [11].

Reactive element oxides and perovskite ceramics were considered as the coatings [12–14], which may improve scale adhesion and reduce the growth rate of oxide scales; however, they are not favored because of their high sintering temperature for coating formation, unacceptably high electrical resistance, incompatibility with the thermally grown oxides or instability in SOFC anode environment [10,11]. It has been also realized that coatings containing Cr element may not be able to effectively alleviate the issue of cathode poisoning caused by Cr evaporation. Therefore, recent attentions have been paid to spinel coatings that contain no Cr element, such as Mn–Co [4,15,16], Mn–Cu [17] spinels. They were proved to decrease the growth of Cr_2O_3, increase the electronic conductivity of the oxide scales, and possibly suppress the formation of volatile Cr-containing species.

$NiMn_2O_4$, containing no Cr element, is a conventional material for thermistors with a negative temperature coefficient. Its conductivity is determined by electron hopping between Mn^{3+} and

* Corresponding author. Tel.: +86 27 87558142; fax: +86 27 87558142.
E-mail address: pujian@hust.edu.cn (J. Pu).

0378-7753/$ – see front matter © 2011 Elsevier B.V. All rights reserved.
doi:10.1016/j.jpowsour.2011.02.075

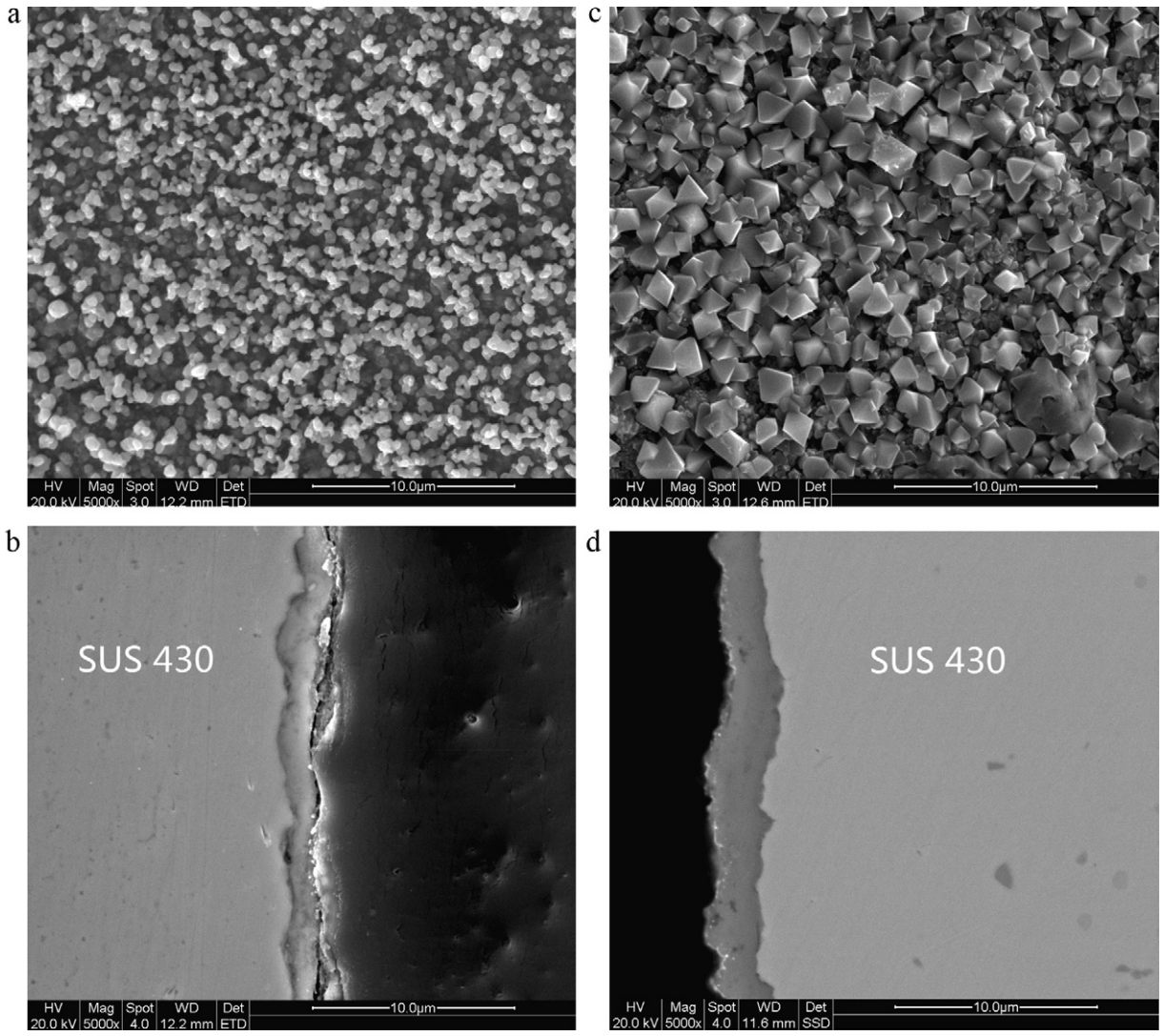

Fig. 1. Surface morphology and cross-section of the as-coated and subsequently oxidized SUS 430 specimens, the cyclic oxidation was performed at 750 °C in air for 1000 h: (a) surface of the as-coated; (b) cross-section of the as-coated; (c) surface of the oxidized; and (d) cross-section of the oxidized.

Mn^{4+} cations located in the octahedral sites of the spinel structure, and is equivalent to that of $MnCo_2O_4$ [18]. The cost of $NiMn_2O_4$ is significantly lower than that of $MnCo_2O_4$ as it contains no Co element; therefore, it is suitable as a candidate coating material for the metallic interconnects. In the present study, spinel $NiMn_2O_4$ was used as the coating material on SUS 430 stainless steel substrate for the application of the metallic interconnects, and the effect of $NiMn_2O_4$ coating prepared by the sol–gel process on the oxidation resistance and the ASR of the coated SUS 430 stainless steel was evaluated.

2. Experimental

SUS 430 ferritic stainless steel, containing 16.76 wt% Cr, 0.69 wt% Mn, 0.75 wt% Si, 0.12 wt% C, was used as the substrate on which $NiMn_2O_4$ coating was applied. Rectangular coupons with dimensions of 25 mm × 25 mm × 1 mm were cut from sheet SUS 430, mechanically polished with SiC papers up to 400-grit and ultrasonically cleaned prior to coating. The sol–gel solution for making $NiMn_2O_4$ spinel was prepared by dissolving nickel chloride hexahydrate ($NiCl_2{\cdot}6H_2O$) and manganese chloride ($MnCl_2$) in 1–2 molar ratio into ethylene glycol with citric acid monohydrate as the chelating agent. Dipping process was utilized to coat the coupons with the solution; and the coated coupons were dried in an oven at 80–120 °C. In order to form the phase $NiMn_2O_4$, the dried coupons were slowly heated up and held at 750 °C in an atmosphere controlled furnace under a reducing atmosphere 5% H_2 + 95% N_2 for 2 h and subsequently under air for another 2 h to prevent significant oxidation of the substrate alloy during coating formation [4].

The oxidation behavior of the coated SUS 430 coupons was characterized by cyclic oxidation. The samples was oxidized at 750 °C in air for 100 h and then cooled in air to room temperature. This procedure was repeated 10 times (10 thermal cycles) for an accumulated oxidation time of 1000 h. The weight gain after each thermal cycle was recorded by using a Sartorius BT-25S electronic balance with an accuracy of 10^{-5} g.

A PANalytical X'Pert PRO X-ray diffractometer (XRD) with Cu Kα radiation was used for phase identification of the coating and oxide scale. A FEI Quanta 200 scanning electron microscope (SEM) equipped with an energy dispersive spectrometer (EDS) was employed for microstructure examination and composition analysis. The electrical resistance of the oxidized samples was measured using the conventional four-probe DC technique, as described in detail in Ref. [19], at temperatures from 500 to 800 °C in air.

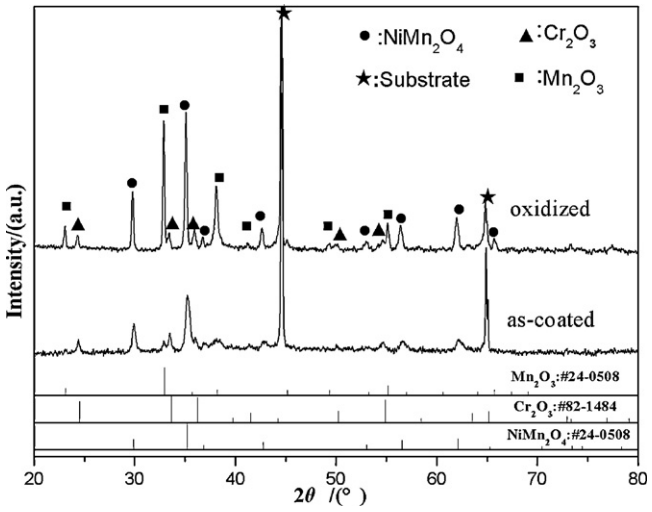

Fig. 2. XRD patterns of the as-coated and subsequently oxidized SUS 430 alloy, in comparison with ICCD files for $NiMn_2O_4$, Cr_2O_3 and Mn_2O_3 phases. The oxidation was performed cyclically at 750 °C in air for 1000 h.

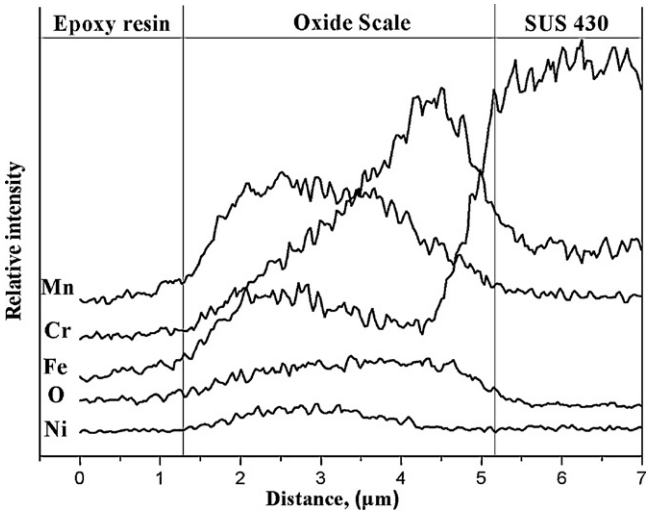

Fig. 3. EDS compositional profile crossing the thickness of the oxide scale formed on the $NiMn_2O_4$ coated SUS 430 alloy in cyclic oxidation at 750 °C in air for 1000 h, showing Cr distribution in the area adjacent to the substrate and Fe, Mn and Ni distributions in the rest area of the scale.

3. Result and discussions

Fig. 1 shows the surface morphology and the cross-section of the as-coated and oxidized SUS 430 coupons. Before the long-term oxidation, the top surface of the coating is featured with loosely packed fine oxide particles (Fig. 1a); however, the coating is dense underneath with a thickness of 1–2 μm (Fig. 1b) and well adhered to the substrate. After 1000 h cyclic oxidation at 750 °C in air, the surface oxide became largely grained and densely packed (Fig. 1c), and the oxide scale increased to 3–4 μm thick and maintained adhesion to the substrate (Fig. 1d).

Fig. 2 demonstrates the XRD patterns of the as-coated SUS 430 specimen and that subsequently oxidized at 750 °C in air for 1000 h, in comparison with the ICDD (International Center for Diffraction Data) files for $NiMn_2O_4$, Cr_2O_3 and Mn_2O_3. In the case of the as-coated one, in addition to the diffraction peaks generated from the substrate SUS 430 alloy, the rest of the diffraction pattern matches to the files of $NiMn_2O_4$, Cr_2O_3 and Mn_2O_3. The primary phase in the coated oxide scale is $NiMn_2O_4$, which was transformed from the sol–gel coating; and the minor phases are Cr_2O_3 and Mn_2O_3, which were formed from the substrate alloy during the process of pre-oxidation for coating formation. As known, Cr and Mn are less noble than Fe and are prone to be oxidized selectively. In the period of oxidation at 750 °C in air up to 1000 h, the thickness of the oxide scale increased with time; however, the type of phases in the scale remained similar to those prior to the long-term oxidation, and basically $NiMn_2O_4$, Cr_2O_3 and Mn_2O_3 were identified, as indicated in Fig. 2. It is found by closely comparing the diffraction pattern and the ICCD files that the diffraction peaks generated from the $NiMn_2O_4$ and Cr_2O_3 phases are slightly left-shifted from the ICCD files, which suggests that they are not pure $NiMn_2O_4$ and Cr_2O_3 anymore and possibly doped by other elements. For $NiMn_2O_4$, the possible doping elements here are Fe and Cr; and for Cr_2O_3, are Fe and Mn. According to the ion radii of the possible doping elements [20], it is probable that the $NiMn_2O_4$ was partially doped by Fe and/or Cr at either the Ni or Mn sites, and the Cr_2O_3 was partially doped by Mn. It also can be seen from Fig. 2 that the diffraction intensity of the Mn_2O_3 and doped $NiMn_2O_4$ is considerably increased after the long-term cyclic oxidation, whereas that of the doped Cr_2O_3 remained unchanged. This suggests that the growth of Cr_2O_3 was effectively suppressed by the coating.

Fig. 3 shows the element distribution across the oxide scale formed during the 1000 h cyclic oxidation. Cr is spread in the area adjacent to the substrate, while Ni, Mn and Fe are distributed in the area close to the surface. This result confirms that the doped Cr_2O_3 oxide is covered by the doped $NiMn_2O_4$ and Mn_2O_3 oxides and no Cr-containing species is exposed directly to air. Comparing to the oxide scale thermally grown on the uncoated SUS 430 alloy, on top of which Cr_2O_3 flakes and $MnCr_2O_4$ spinel grains are presented [4], such formed oxide scale is expected to be a barrier to Cr outward diffusion and alleviate the cathode poisoning caused by the evaporation of Cr_2O_3 from the oxide scale to form volatile Cr-containing species in SOFC cathode atmosphere. From the appearance, it is hard to distinguish between the doped $NiMn_2O_4$ and Mn_2O_3 in Fig. 1c as they both are cubic in crystal structure; however, Mn_2O_3 may appear in the top layer of the oxide scale due to the fast outward diffusion rate of Mn ion [21–23]. The distribution of Fe element is consistence with that of Mn element across the thickness of the oxide scale, which implies that both $NiMn_2O_4$ and Mn_2O_3 were doped by Fe, as suggested by the XRD result in Fig. 2.

Fig. 4 shows the weight gain of the cyclic oxidation at 750 °C in air as a function of oxidation time for the $NiMn_2O_4$ coated SUS 430 alloy, in comparison with those obtained with un-coated and Mn–Co spinel coated 430 alloys. The oxidation kinetics obeys

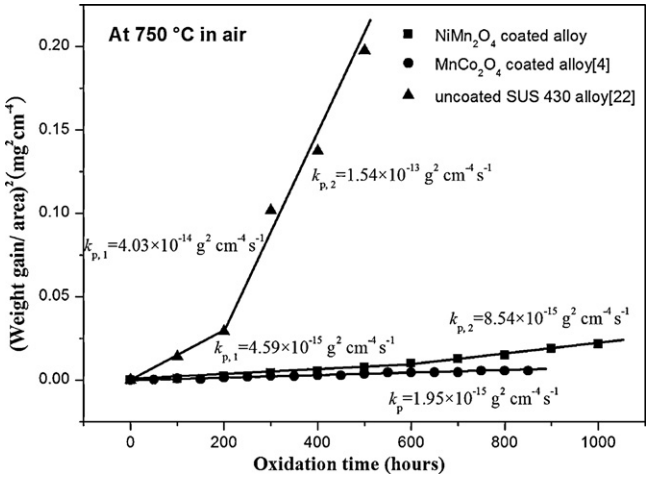

Fig. 4. Oxidation weight gain of the $NiMn_2O_4$ coated SUS 430 alloy as a function of cyclic oxidation time at 750 °C in air, in comparison with the uncoated and Mn–Co spinel coated 430 alloys.

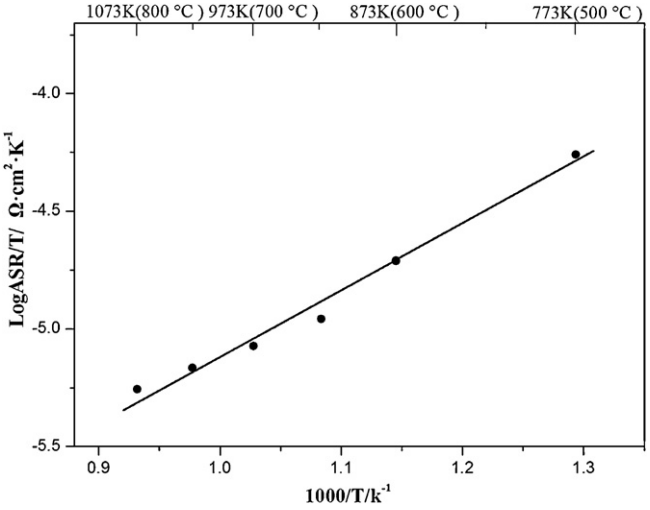

Fig. 5. Dependence of ASR of the $NiMn_2O_4$ coated and oxidized SUS 430 alloy as a function of measurement temperature. The oxidation was performed cyclically at 750 °C in air for 1000 h.

approximately the parabolic rate law with two rate constants as observed previously [22], i.e. $4.59 \times 10^{-15}\,g^2\,cm^{-4}\,s^{-1}$ for oxidation in the period of 0–600 h and $8.54 \times 10^{-15}\,g^2\,cm^{-4}\,s^{-1}$ for 600–1000 h. The slight increase may be caused by accelerated Mn outward diffusion from the substrate through the oxide scale to form Mn_2O_3 on the top surface; however, such rate constant increase is expected to diminish with further oxidation soon after Mn depletion occurs in the substrate near the substrate/scale interface [24]. These two rate constants are comparable with that obtained with $MnCo_2O_4$ coated SUS 430 alloy [4] and significantly lower than the rate constant of uncoated SUS 430 alloy [22], which proves the effectiveness of $NiMn_2O_4$ coating as a barrier to oxidation by inhibiting Cr outward diffusion and oxygen inward diffusion to thicken Cr_2O_3 and form $MnCr_2O_4$. Fig. 5 is the Arrhenius plot of area specific resistance (ASR) contributed by the oxide scale formed during the 1000 h cyclic oxidation. Log(ASR/T) is linearly proportional to 1/T, showing the electrical behavior of semi-conductors. In the temperature range of 600–800 °C, the ASR is from 6 to 17 $m\Omega\,cm^2$, which is about two orders of magnitude lower than that of the uncoated SUS 430 alloy and equivalent to that of $MnCo_2O_4$ coated SUS 430 alloy oxidized at 750 °C in air for 850 h [25]. At 750 °C, the ASR is 7 $m\Omega\,cm^2$, the ohmic loss associated with the ASR at conventional current density 0.5 $A\,cm^{-2}$ is only 3.5 mV. Such a low ASR is attributed to the higher electrical conductivity of both $NiMn_2O_4$ and Mn_2O_3 than that of Cr_2O_3 and $MnCr_2O_4$. This once again demonstrates that $NiMn_2O_4$ is an excellent coating material for metallic interconnects of the intermediate temperature SOFCs.

4. Conclusions

The effectiveness of sol–gel derived $NiMn_2O_4$ coating was evaluated in air at 750 °C as a protective barrier to oxidation for the SUS 430 alloy as a metallic interconnect material of the intermediate temperature SOFCs, and the following conclusions can be made based on the obtained results.

(1) Sol–gel method is a convenient method to generate a $NiMn_2O_4$ spinel coating on SUS 430 alloy. A well crystallized, adhesive and dense $NiMn_2O_4$ coating with a thickness of 1–2 μm can be obtained by dip-coating, followed by heat treatment at temperatures up to 750 °C.

(2) The oxide scale of the $NiMn_2O_4$ coated SUS 430 alloy formed in 1000 h cyclic oxidation at 750 °C in air consists of an inner layer of Mn- and/or Fe-doped Cr_2O_3 and an outer layer of Fe-doped $NiMn_2O_4$ and Mn_2O_3. The growth of Cr_2O_3 and formation of $MnCr_2O_4$ are effectively depressed by the presence of Cr-free $NiMn_2O_4$ and Mn_2O_3 oxides, which is expected to alleviate the cathode poisoning by Cr evaporation.

(3) The oxidation resistance of SUS 430 alloy is significantly increased by the $NiMn_2O_4$ coating; and the kinetics of cyclic oxidation at 750 °C in air for up to 1000 h obeys the parabolic low with two rate constant of $4.59 \times 10^{-15}\,g^2\,cm^{-4}\,s^{-1}$ (0–600 h) and $8.54 \times 10^{-15}\,g^2\,cm^{-4}\,s^{-1}$ (600–1000 h). The ASR of such formed oxide scale is 7 $m\Omega\,cm^2$ at 750 °C in air, which demonstrates that $NiMn_2O_4$ is an excellent coating material for metallic interconnects of the intermediate temperature SOFCs.

Acknowledgements

This research was financially supported by the National "863" Program (No. 2006AA03Z227) and the National Natural Science Foundation of China (No. 50771048). The SEM and XRD characterizations were assisted by the Analytical and Testing Center of Huazhong University of Science and Technology.

References

[1] Z.G. Yang, Int. Mater. Rev. 53 (2008) 39–54.
[2] W.Z. Zhu, S.C. Deevi, Mater. Res. Bull. 38 (2003) 957–972.
[3] J.W. Fergus, Mater. Sci. Eng. A397 (2005) 271–283.
[4] B. Hua, J. Pu, W. Gong, J.F. Zhang, F.S. Lu, L. Jian, J. Power Sources 185 (2008) 419–422.
[5] D.E. Alman, P.D. Jablonski, Int. J. Hydrogen Energy 32 (2007) 3743–3753.
[6] M. Stanislowski, E. Wessel, K. Hilpert, T. Markus, L. Singheiser, J. Electrochemical. Soc. 154 (2007) A295–A306.
[7] Z.G. Yang, G.G. Xia, X.H. Li, J.W. Stevenson, Int. J. Hydrogen Energy 32 (2007) 3648–3654.
[8] W.Z. Zhu, S.C. Deevi, Mater. Sci. Eng. A348 (2003) 227–243.
[9] J.W. Fergus, Int. J. Hydrogen Energy 32 (2007) 3664–3671.
[10] M. Stanislowski, J. Froitzheim, L. Niewolak, W.J. Quadakkers, K. Hilpert, T. Markus, L. Singheiser, J. Power Sources 164 (2007) 578–589.
[11] N. Shaigan, W. Qu, D.G. Ivey, W. Chen, J. Power Sources 195 (2010) 1529–1542.
[12] W. Qu, J. Li, D.G. Ivey, J. Power Sources 138 (2004) 162–173.
[13] W. Qu, J. Li, D.G. Ivey, J.M. Hill, J. Power Sources 157 (2006) 335–350.
[14] J.-H. Kim, R.-H. Song, S.-H. Hyun, Solid State Ionics 174 (2004) 185–191.
[15] C.C. Mardare, M. Spiegel, A. Savan, A. Ludwig, Int. J. Hydrogen Energy 156 (2009) B1431–B1439.
[16] J.W. Wu, C.D. Johnson, Y.L. Jiang, R.S. Gemmen, X.B. Liu, Electrochim. Acta 54 (2008) 793–800.
[17] M.R. Bateni, P. Wei, X. Deng, A. Petric, Surf. Coat. Technol. 201 (2007) 4677–4684.
[18] M. Vakiv, O. Shpotyuk, O. Mrooz, I. Hadzaman, J. Eur. Ceram. Soc. 21 (2001) 1783–1785.
[19] B. Hua, J. Pu, J.F. Zhang, F.S. Lu, B. Chi, L. Jian, J. Electrochem. Soc. 156 (2009) B93–B98.
[20] R.D. Shannon, Acta Cryst. A32 (1976) 751–767.
[21] B. Hua, J. Pu, F.S. Lu, J.F. Zhang, B. Chi, L. Jian, J. Power Sources 195 (2010) 2782–2788.
[22] J. Pu, J. Li, B. Hua, G. Xie, J. Power Sources 158 (2006) 354–360.
[23] Z.G. Yang, J.S. Hardy, M.S. Walker, G.G. Xia, S.P. Simmer, J.W. Stevenson, Int. J. Hydrogen Energy 151 (2004) A1825–A1831.
[24] J. Li, J. Pu, B. Hua, G. Xie, J. Power Sources 159 (2006) 641–645.
[25] B. Hua, Y.H. Kong, F.S. Lu, J.F. Zhang, J. Pu, J. Li, Chin. Sci. Bull. 55 (2010) 3831–3837.